Nanoscale electronic transport at graphene/pentacene van der Waals interface.

Michel Daher Mansour[1], Jacopo Oswald[2,3], Davide Beretta[2], Michael Stiefel[2,§], Roman Furrer[2], Michel Calame[2,3,4], Dominique Vuillaume[1].

1. Institut for Electronic, Microelectronic and Nanotechnology, Centre National de la Recherche Scientifique, Villeneuve d'Ascq, France.
2. Transport at Nanoscale Interfaces Laboratory, Swiss Federal Laboratories for Material Science and Technology (EMPA), Dübendorf , Switzerland.
3. Swiss Nanoscience Institute, University of Basel, Switzerland.
4. Department of Physics, University of Basel, Switzerland.

§ Current address : IBM, Binnig and Rohrer Nanotechnology Center, Zurich, Switzerland.

* Corresponding authors: dominique.vuillaume@iemn.fr; michel.calame@empa.ch

Supporting Information

1. Metal electrodes on Si/SiO_2.

Ti (5nm) / Au (50 nm) electrodes were fabricated on a 4-inch Si (525 µm thick) / SiO_2 (285 nm thick) wafer, which was pre-cleaned in oxygen plasma (600 W for 5 min). The electrodes (Ti/Au) were deposited by e-beam physical vapor deposition (EBPVD) and patterned by liftoff in DMSO (dimethyl sulfoxide) at 100°C for 30 min. The resist for the liftoff (AZ2020nlof) was spin-coated (4000 rpm for 60 s),

exposed to UV light (lamp intensity 11 mW/cm^2) through an optical mask, and then developed (AZ726mif, 35 s).

2. CVD graphene, transfer protocol and characterizations.

Graphene was grown in-house by chemical vapor deposition (CVD) on copper foils. The growth protocol can be found in previously reported works.[1-3] CVD graphene foil (Cu/Gr/PMMA) was placed to float in a copper etchant (Transene CE-100) for 1h, the PMMA layer facing upwards. Once the copper is completely etched (Gr/PMMA), the etchant was removed and replaced with deionized water, twice. Then, the foil was transferred to a 10% HCl cleaning solution for 5 min and transferred back to deionized water, twice. The floating graphene foil (Gr/PMMA) was transferred onto the substrate (Si/SiO_2/Ti/Au/Gr/PMMA) and let dry in air for 1 h. The chip was annealed overnight at 80°C in the vacuum (~1 mbar). Finally, the PMMA is removed in acetone (45 min at 50°C). Fig. S1 shows the TM-AFM of the deposited Gr flakes and after annealing at 150°C and 450°C (3h under N_2).

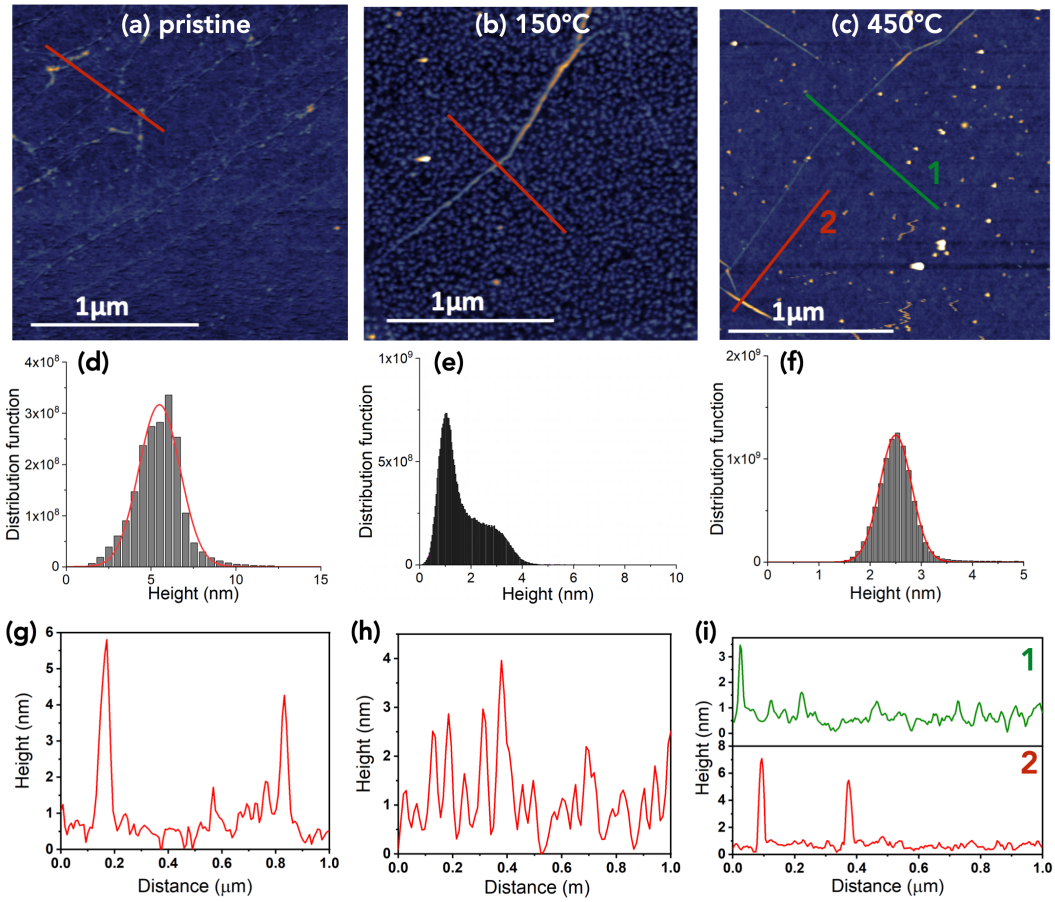

Figure S1. *TM-AFM images of Gr flakes: (a) after transfer onto SiO_2, (b) annealed at 150°C and (c) annealed at 450°C. (d-f) Corresponding histograms of heights (the red lines are Gaussian fits) and (g-i) typical profiles along the lines shown in panels (a-c).*

These measurements show a clear removal of PMMA residues after the annealing at 450°C as indicated by a significant decrease of the width of the height distribution (2.9 nm FWHM for the as-deposited Gr and 0.7 nm for the Gr flake annealed at 450°C). The PMMA removal is incomplete after the annealing at 150°C (FWHM of 0.74 nm for the main peak, but a larger shoulder is still visible). Wrinkles are still present after the annealing. The calculated rms roughness (masking the wrinkles and the brighter spots probably corresponding to dust

since the AFM measurements were done in air) decrease from 2.7 nm for the as-transferred Gr to 1.8 nm after a 150°C annealing and 0.7 nm after a 450°C annealing. The reduction of roughness and height distribution FWHM indicates the removal of PMMA residues from the Gr surface (only incomplete for the annealing at 150°C) and thus a cleaner and smoother surface, which is mandatory to grow the OSC molecules.

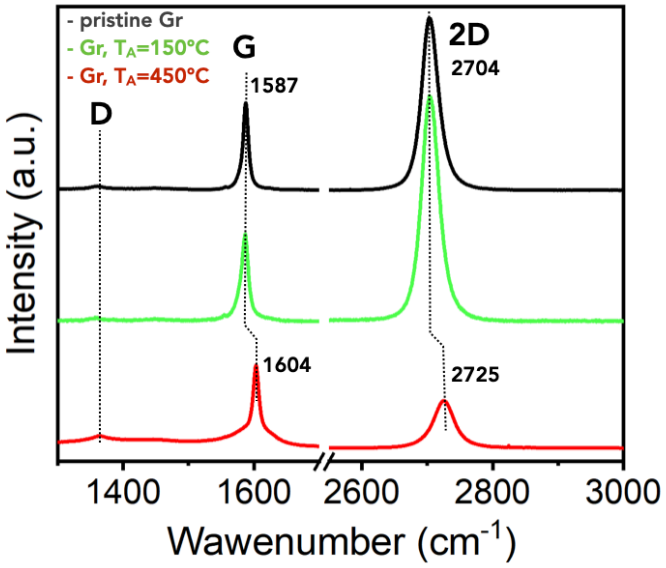

***Figure S2**. Raman spectra (D, G and 2D peaks) of the Gr flakes after deposition and annealing at 150 and 450°C.*

Fig. S2 shows the Raman spectra of graphene. The annealing at 150°C does not induce significant change. The values of the G and 2D peaks (at 1587 cm^{-1} and 2704 cm^{-1}, respectively) slightly higher than the expected values for a neutral Gr indicates a weak residual hole doping.[4, 5] We can estimate the Gr charge density, n, from the relations:[4, 6]

$$\omega_G - \omega_G^0 = (42\ cm^{-1}/eV)\left|\varepsilon_F\right| \ ;\ \varepsilon_{DP} - \varepsilon_F = sgn(n)\hbar v_F\sqrt{\pi\,|n|} \qquad \text{(S1)}$$

with ω_G the G peak position, ω_G^0 = 1580 cm^{-1} for the undoped Gr,[4] ε_F the Fermi energy and ε_{DP} the energy of the Dirac point, ħ the reduced Planck constant and υ_F the graphene Fermi velocity ~10^6 m/s. With ω_G = 1587 cm^{-1}, we get $\varepsilon_{DP} - \varepsilon_F$ = 170 meV and a hole density n = 1.6x10^{12} cm^{-2}.

The treatment at 450°C leads to a blue shift of the graphene peaks. The, G and 2D peaks (at 1587 cm^{-1} and 2704 cm^{-1}, respectively for the as-transferred Gr and annealed at 150°C) shifted toward higher wavenumbers by ~21 cm^{-1} and ~17 cm^{-1}, respectively, for the Gr flakes annealed at 450°C. The intensity ratio 2D/G also decreases from ~2-2.5 (pristine Gr and annealed at 150°C) to ~0.6 after annealing at 450°C, indicating an additional hole doping of the 450°C annealed Gr,[5, 7, 8] likely due to the thermal activation of electron transfer from Gr to the substrate.[9] With Eq. S1, we get $\varepsilon_{DP} - \varepsilon_F$ = 550 meV and a hole density n = 1.8x10^{13} cm^{-2}. In all cases, the intensity of the D peak remains low (no defect induced in the Gr).

3. Pentacene evaporation.

The purified pentacene (99.999 %), purchased from Tokyo Chemical Industry (TCI), is sublimated by Joule heating (crucible temperatures 90-120°C) in a 10^{-6} mbar vacuum evaporation system (Edwards Auto306) placed inside a glovebox (MBRAUN, H_2O and O_2 levels below 5 ppm). The deposition rate and time (typically ≈ 2.5x10^{-3} Å/s, ≈ 30 min) were adjusted to grow the desired nanostructure from few MLs to bulky films: dendritic islands of pentacene with thicknesses lower than 10 nm were obtained when P5 was evaporated at 2.5x10^{-3} Å/s for 30 mins on Gr annealed at 150°C. At the same rate, needle-like P5 islands with thicknesses ranging from 15 nm to 30 nm were obtained on Gr annealed at a temperature of 450°C. For bulk films (400 nm), see below, the rate was changed to 0.1 Å/s for 1hr. The substrate is kept at room temperature.

4. Macroscopic Gr/P5 device.

The growth of a 400 nm thick P5 film was achieved via the evaporation of P5 through a mechanical mask. After the process described in section 2, we fix, on a sample holder, a mask with openings of 100x100 μm^2 in front of the sample. The shadow mask is held in an aligned way with the sample that allows the growth of thin films on specific locations on the Gr/SiO_2/Si surface (optical image in the inset of Fig. S3).

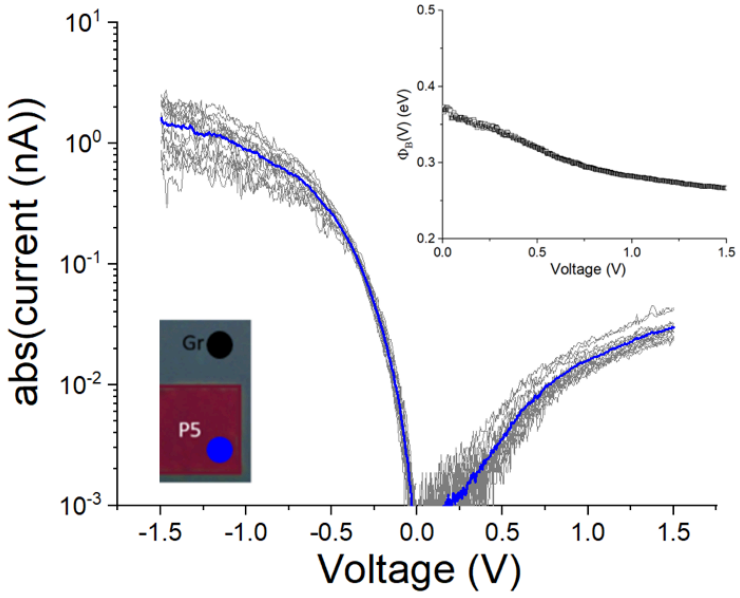

***Figure S3**. I-V data set (gray curves, 16 I-V traces, C-AFM measurements) and mean Ī-V (blue curve) of P5 thin film, 400 nm thick, grown on Gr flake annealed at 150°C. The inset (down left) shows an optical image of the 100 µm x 100 µm P5 film and the underlying Gr flake. Inset (up right) : Voltage dependent energy barrier height for the macroscopic Gr/P5 diode.*

The I-V in Fig. S3 cannot be explained by the DSB model, because the high current at V<0 cannot correspond to the saturation current of the P5/PtIr tip diode with a tiny (~15 nm^2) surface (even with a very small Schottky barrier

height), while the lower current at V>0 corresponds to the saturation current of the large area (100µm x 100µm) Gr/P5 diode, as for the 15-30 nm N-like P5 samples (Figs. 8, S10). Consequently, we assume that only the Gr/P5 diode is measured for this macroscopic sample, the current at V>0 being the forward current of this diode, as also reported for macroscopic P5/Gr diodes (with lithographed top electrodes).[10-13] For the reverse bias (V>0), we considered a modified thermionic emission (MTE) model that takes into account the dependence of the Gr Fermi level with the applied voltage and allow to explain the voltage-driven increase of the saturation current in the reverse regime (V>0).[14, 15] The saturation current I_S is written:

$$I_S = AA^*T^2e^{-\Phi_B(V)/kT} \quad \text{(S2)}$$

with A the contact area, A* the Richardson constant, k the Boltzmann constant, T the temperature and $\Phi_B(V)$ the voltage-dependent Schottky barrier height (SBH) at the Gr/OSC interface. From the mean $\bar{I}$-V, we plot (inset) $\Phi_B(V) = -kTLn(I_S/AA^*T^2)$. The zero bias SBH value $\Phi_{B0} \approx 0.38$ eV and the voltage variations of $\Phi_B(V)$ are in agreement with the reported values for macroscopic Gr/P5 diodes (~ 0.25-0.5 eV) with lithographed top electrodes.[10, 11, 16]

5. C-AFM method

5.1. Discarded I-V traces.

Some I-V curves were discarded from the analysis:

- I-V traces displaying large and abrupt steps during the scan (contact instabilities).
- At low currents, the I-V traces that reached the sensitivity limit (almost flat I-V traces and noisy I-Vs) and displayed random staircase behavior (due to the sensitivity limit - typically 0.1-1 pA depending on the used gain of the trans-impedance amplifier and the resolution of the ADC (analog-digital converter).

Typical examples are shown in Fig. S4.

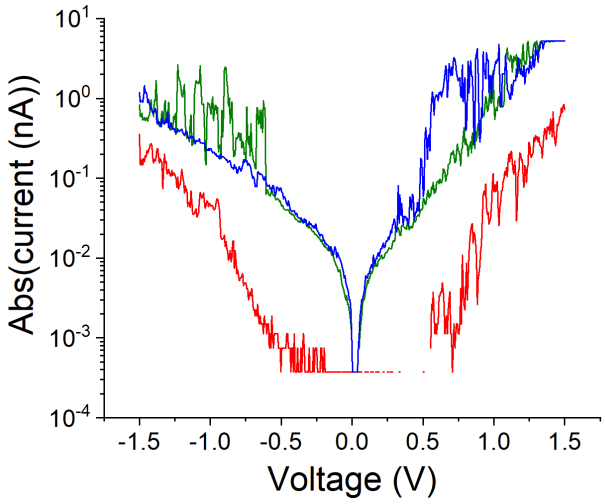

Figure S4. *Three typical I-V traces discarded from the analysis (sample A, 30 nm thick P5 nanostructure).*

5.2. Estimated C-AFM tip contact area and number of contacted molecules.

The loading force was set at ~ 8 nN for all the I-V measurements, a lower value leading to too many contact instabilities during the I-V measurements. As usually reported in literature[17-20] the contact radius, r_c, between the CAFM tip and the P5 surface, and the film elastic deformation, δ, are estimated from a Hertzian model:[21]

$$r_c^{\,2} = \left(\frac{3RF}{4E^*} \right)^{2/3} \qquad \text{(S3)}$$

$$\delta = \left(\frac{9}{16R} \right)^{1/3} \left(\frac{F}{E^*} \right)^{2/3} \qquad \text{(S4)}$$

with F the tip loading force (8 nN), R the tip radius (25 nm) and E* the reduced effective Young modulus defined as:

$$E^* = \left(\frac{1}{E^*_{P5}} + \frac{1}{E^*_{tip}} \right)^{-1} = \left(\frac{1-\nu^2_{P5}}{E_{P5}} + \frac{1-\nu^2_{tip}}{E_{tip}} \right)^{-1} \quad \text{(S5)}$$

In this equation, $E_{P5/tip}$ and $\nu_{P5/tip}$ are the Young modulus and the Poisson ratio of the P5 and C-AFM tip, respectively. For the Pt/Ir (90%/10%) tip, we have E_{tip} = 204 GPa and ν_{tip} = 0.37 using a rule of mixture with the known material data (https://www.webelements.com/). For the P5 nanostructures, we consider the value of an effective Young modulus E^*_{P5} = 15 GPa as measured for thermally evaporated P5.[22, 23] With these parameters, we estimate $r_c \approx 2.2$ nm (contact area ≈ 15 nm^2) and $\delta = 0.19$ nm.

In a P5 film, the molecules (in the upright position) are organized in stacked monolayers with a herringbone packing in the monolayer and an area per molecule of ≈ 0.25 nm^2. We estimate that ≈ 60 P5 molecules are connected with the C-AFM tip with our measurement condition.

6. Graphene resistance.

The graphene series resistance (graphene in-plane resistance and contact resistance) was measured with the graphene layer connected between two lithographed electrodes separated by a length L = 100µm and width W = 200 µm on a 285 nm thick SiO_2 (see section 1 of the SI). Figure S5 shows the typical I-V at low voltages. From the linear behavior, we measured a series resistance of 285 Ω. Rescaled to the typical geometry of the P5 islands measured by C-AFM (Figs. 4 and 5, main text) with a typical length L ~ 10 µm between the P5 island and the nearest electrode (see Fig. 4-a, main text) and a typical width of the P5 islands of W ~ 1 µm, the series resistance in the C-AFM geometry is ~ 5 kΩ.

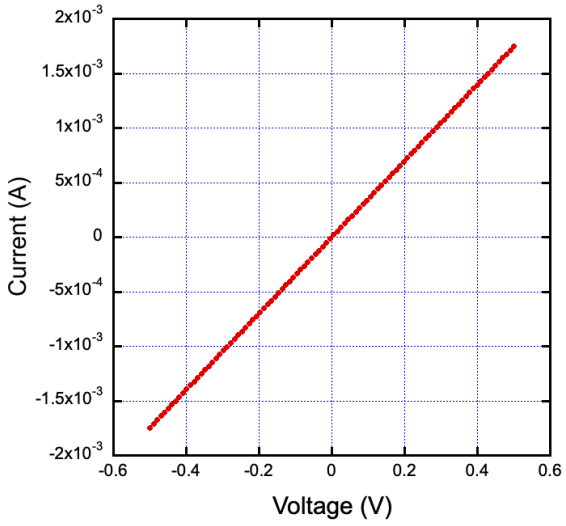

Figure S5. *Current vs. voltage to measure the series resistance (graphene resistance and contact resistance).*

7. Details of the models.

Molecular 2-site model.

In Eq. (1), the parameters ε_{1*} and ε_{2*} are defined by : $\varepsilon_{1*} = (\varepsilon_1 + \varepsilon_2 - \Delta)/2$, $\varepsilon_{2*} = (\varepsilon_1 + \varepsilon_2 + \Delta)/2$ and Δ is the energy shift between the two orbitals under the application of a voltage V given by $\Delta=(V_i^2+2(\varepsilon_1-\varepsilon_2)V_i+4\tau^2+(\varepsilon_1-\varepsilon_2)^2)^{1/2}$.[24, 25]

In Eq. (2), the internal voltage drop in graphene between the Dirac point and the Fermi energy, $\delta(V)$, is calculated versus the applied voltage V according to Feenstra et al. [26] and given by

$$\delta(V) = \pm\frac{1}{2}\left[\frac{-2C\pi\left(\hbar v_F\right)^2}{e^2} + \sqrt{\left[\frac{2C\pi\left(\hbar v_F\right)^2}{e^2}\right]^2 \pm 4\pi\left(\hbar v_F\right)^2\left(n_0 + \frac{CV}{e}\right)}\right] \quad \text{(S6)}$$

with $\hbar$ the reduced Planck constant, v_F the graphene Fermi velocity (≈ 10^6 m/s), n_0 the intrinsic Gr doping at 0 volt and C the capacitance of the sample (the upper plus sign for $V>-en_0/C$ and the lower minus sign for $V<-en_0/V$), see Fig. S6. We have measured n_0 = 1.6 x 10^{12} cm^{-2} (see section 2 in this Supporting Information, i.e. at 0 V, ε_{DP} at 170 meV with respect of Fermi energy) and C =

$\varepsilon_{P5}\varepsilon_0/d_{P5} \approx 8x10^{-7}$ F/cm² ($\varepsilon_{P5} \approx 5$, d ≈ 3 nm for 2 layers of P5, ε_0 the vacuum permittivity).

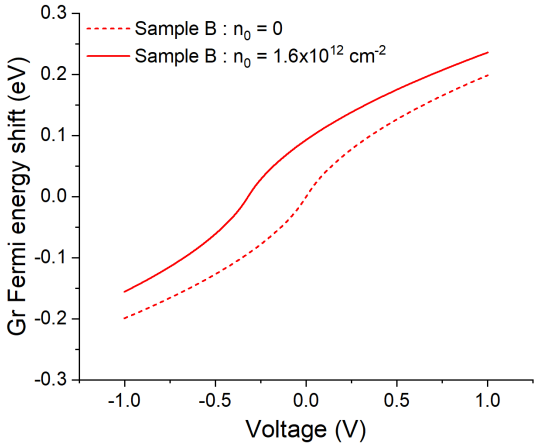

Figure S6. *Typical simulation of Eq. (S6) showing the evolution of the energy difference between the Dirac point and the Fermi level as function of the applied voltage for sample B : no initial doping (dashed line) and with n_0=1.6x10¹² cm⁻².*

Simple fits by parts of the Ī-V curves.

We consider a modified single energy level (SEL) model to take into account the Gr electrode charging with the applied V as above, substituting for Eqs. 2 and S6 in the following SEL equation:[27, 28]

$$I(V) = N\frac{8e}{h}\frac{\Gamma_1\Gamma_2}{\Gamma_1+\Gamma_2}\left[arctan\left(\frac{\epsilon_{1,2}+\frac{\Gamma_1}{\Gamma_1+\Gamma_2}eV_i}{\Gamma_1+\Gamma_2}\right)-arctan\left(\frac{\epsilon_{1,2}-\frac{\Gamma_2}{\Gamma_1+\Gamma_2}eV_i}{\Gamma_1+\Gamma_2}\right)\right] \quad \text{(S7)}$$

where Γ_1 and Γ_2 are now the electronic coupling of the molecule to the two electrodes which are supposed to be different considering the asymmetric geometrical position (Figs. 6d and 6e, main text) of the MO in the junction (while $\Gamma_1 = \Gamma_2 = \Gamma$ in the 2-site model for simplicity).

Case of the 3L data (point #2).

We note that the fit of the 2-site model on the mean $\bar{I}$-V measured at point #2 is a bit worse than at points #1 and #3 (Figs. S8 and S9, R^2=0.984 at #2 vs. 0.995 and 0.991 at #3 and #1, respectively, and a larger overlap of the statistical distributions of ε_1 and ε_2) because there is about 3 P5 layers in that case. Nevertheless, the same trends are observed as for the 2L molecular junctions.

Double Schottky barrier (DSB) vs. 2-site model.

Figure S7 shows that the 2-site molecular model (blue line) does not fit well the data for the N-like P5 nanostructure (here the 30 nm thick). Compared to the DSB model (dashed red line, from Fig. S10), the fit is worse and it gives unrealistic energy level values (*e.g.* ε_1=3.1 eV) larger than the HOMO-LUMO band gap of P5 (2.2 eV).

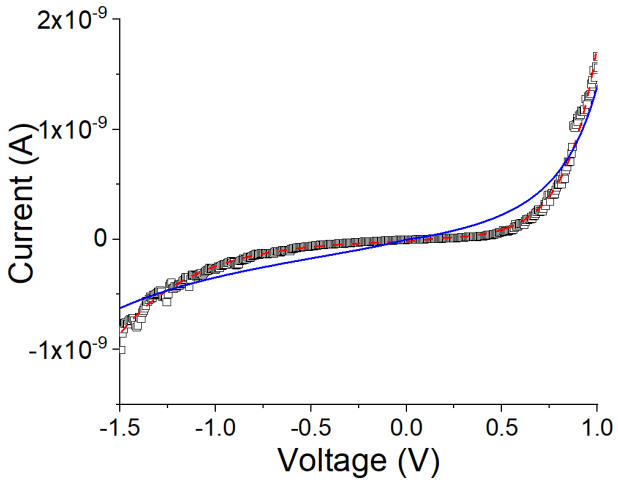

Figure S7. *Fit (blue solid line) of the mean $\bar{I}$-V curve for the 30 nm thick N-like P5 nanostructure (sample A) with the 2-site model. The fit parameters are ε_1=3.1 eV, ε_2=1.1 eV, Γ=0.38 eV and τ=19 meV. For comparison, the dashed red line is the fit with the DSB model (from Fig. S10).*

We also note that the DSB model is not able to correctly fit the data for the few-layers (2L-3L) Gr/P5 devices (sample B) since it is difficult to consider the existence of a space charge region due to the lack of enough room for band

bending in such few-layers devices, albeit several reports pointed out the possibility to use SB model at the nanoscale but with reduced SBH (compared to more bulky devices) because other electron transport mechanisms (*e.g.* tunneling, molecular orbital mediated electron transport) dominate the electron transport at the nanoscale.[29]

8. Fits of the datasets of 2-3 MLs P5 devices at points #1 and #2 (sample B).

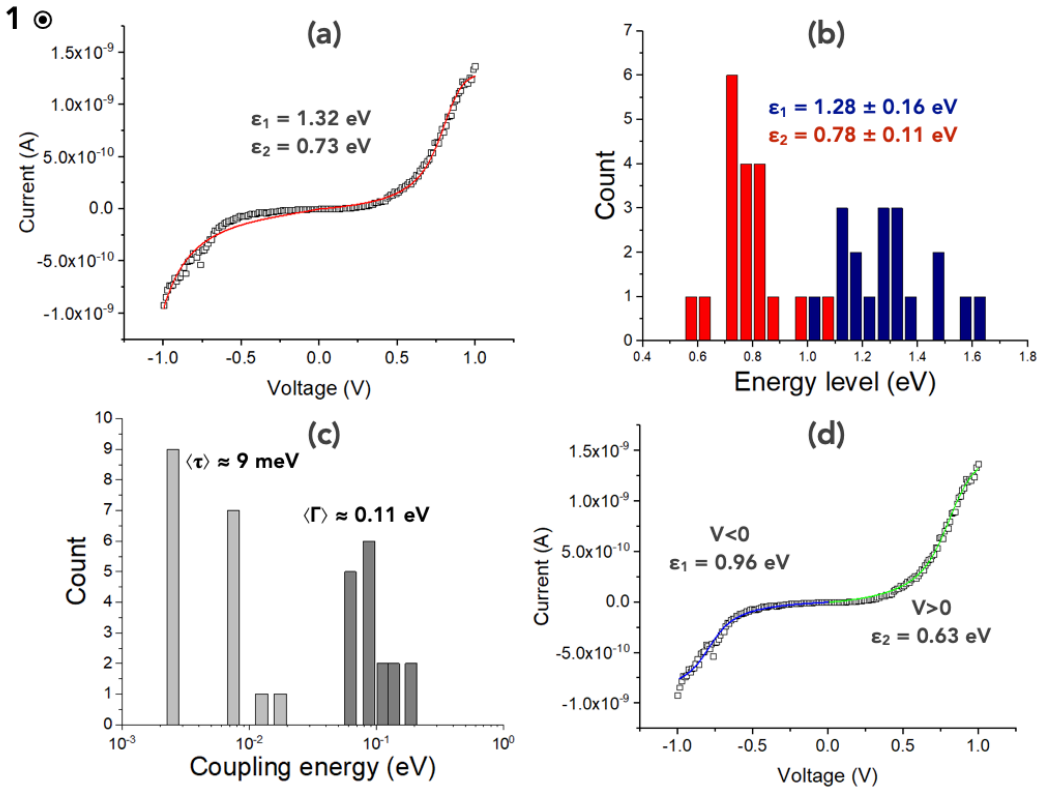

***Figure S8**. Mean Ī-V of the dataset measured at point #1 (from Fig. 5, main text), open black squares: (a) fit (red curve) with the 2-site model taking into account the voltage-induced charging of the Gr layer (Eqs. 1, 2, S6); (b) statistical distribution of the energy levels ε_1 and ε_2 (arithmetic mean ± standard deviation); (c) statistical distribution of the coupling energies Γ, τ (arithmetic mean); (d) fit of the mean Ī-V with the modified SEL (Eq. S7) for the positive voltage (green curve)*

and negative voltage (blue curve). The fitted energy levels of the molecular orbitals (energy scheme in Fig. 6, main text), ε_1 and ε_2, are given on the figures. The other fit parameters (Γ, τ, Γ_1 and Γ_2) are given in Table S1.

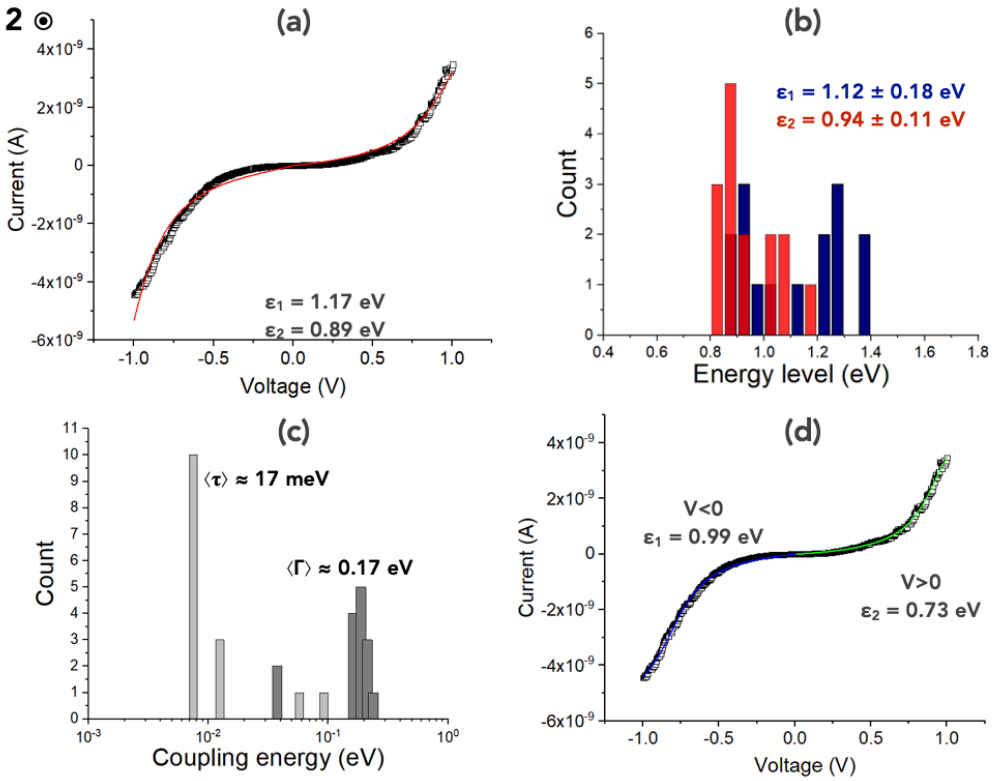

***Figure S9**. Mean $\bar{I}$-V of the dataset measured at point #2 (from Fig. 5, main text), open black squares: (a) fit (red curve) with the 2-site model taking into account the voltage-induced charging of the Gr layer (Eqs. 1, 2, S6); (b) statistical distribution of the energy levels ε_1 and ε_2 (arithmetic mean ± standard deviation); (c) statistical distribution of the coupling energies Γ, τ (arithmetic mean); (d) fit of the mean $\bar{I}$-V with the modified SEL (Eq. S7) for the positive voltage (green curve) and negative voltage (blue curve). The fitted energy levels of the molecular orbitals (energy scheme in Fig. 6, main text), ε_1 and ε_2, are given on the figures. The other fit parameters (Γ, τ, Γ_1 and Γ_2) are given in Table S1.*

		2-site model		SEL (V < 0)	SEL (V>0)
#1	**Γ (eV)** **τ (meV)**	0.11 9	**Γ_1 (eV)** **Γ_2 (eV)**	0.16 ≈ 0	≈ 0 0.14
#2	**Γ (eV)** **τ (meV)**	0.17 17	**Γ_1 (eV)** **Γ_2 (eV)**	0.21 ≈ 0	≈ 0 0.15
#3	**Γ (eV)** **τ (meV)**	0.19 7	**Γ_1 (eV)** **Γ_2 (eV)**	0.22 ≈ 0	≈ 0 0.18

Table S1*. Values of the fitted electronic coupling parameters (see diagrams in Fig. 10) for the 2-site and SEL models (≈ 0 stands for negligible, i.e. < 0.1 meV). With the SEL model, we obtain $\Gamma_1 > \Gamma_2$ at $V < 0$ and $\Gamma_2 > \Gamma_1$ at $V > 0$ as expected from geometrical considerations of the molecular junctions.*

9. Fits of the datasets of the 20 nm and 30 nm thick P5 devices (sample A).

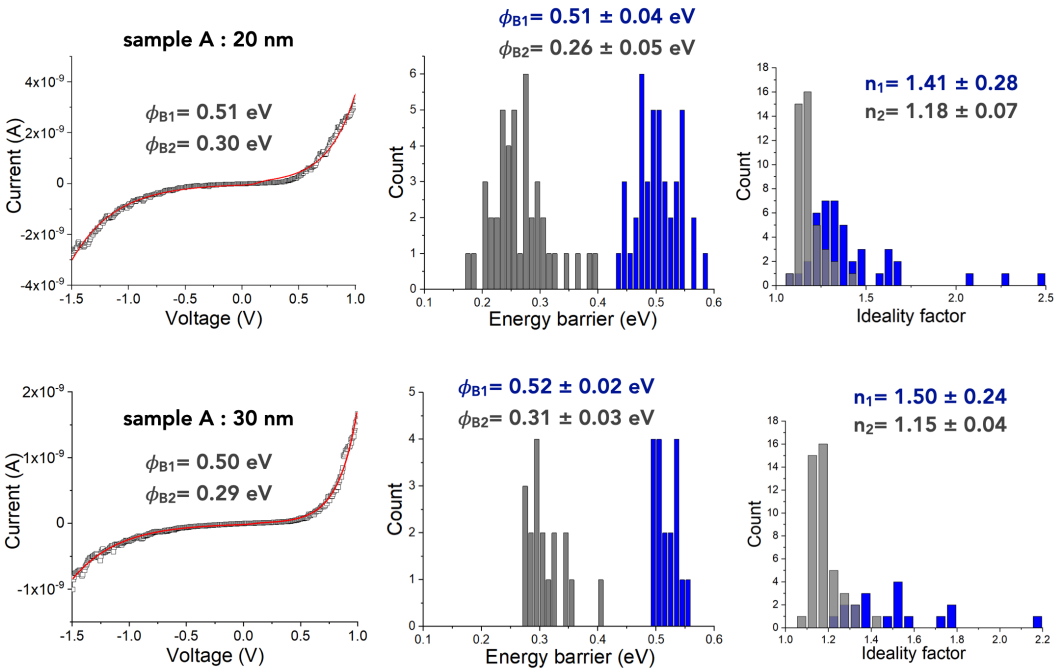

Figure S10. *Fits of the double Schottky diode model on the mean $\bar{I}$-V dataset of sample A. (a) fit (red line) on the mean $\bar{I}$-V (open square, data from Fig. 4, main text) of the 20 nm thick N-like P5 island; (b) statistical distribution of the barrier heights by fitting the model on all the individual I-V traces of the dataset shown in Fig. 4 (main text); (c) statistical distribution of the ideality factors. (d-f) Same as (a-b) for the 30 nm thick N-like P5 nanostructures. Note that for these two samples, the fits were limited to 1V because many I-V traces saturate at V > 1V (compliance of the trans-impedance amplifier, see Figs. 4c and 4d in the main text). All the fit parameters are summarized in Table 2 (main text). For the fits, in Eq. S6, the capacitance C is 2.2×10^{-7} and 1.5×10^{-7} F/cm^2 for the 20 and 30 nm thick P5 nanostructures, respectively, and $n_0 = 1.8 \times 10^{13}$ cm^{-2} (see section 2 in the Supporting Information, i.e. at 0 V, ε_{DP} at 550 meV with respect of the Fermi level).*

References

(1) Braun, O.; Overbeck, J.; El Abbassi, M.; Käser, S.; Furrer, R.; Olziersky, A.; Flasby, A.; Borin Barin, G.; Sun, Q.; Darawish, R.; et al. Optimized graphene electrodes for contacting graphene nanoribbons. *Carbon* **2021**, *184*, 331-339.

(2) Braun, O.; Furrer, R.; Butti, P.; Thodkar, K.; Shorubalko, I.; Zardo, I.; Calame, M.; Perrin, M. L. Spatially mapping thermal transport in graphene by an opto-thermal method. *npj 2D Materials and Applications* **2022**, *6* (1), 6.

(3) Schmuck, O.; Beretta, D.; Furrer, R.; Oswald, J.; Calame, M. A method to fabricate nanoscale gaps in graphene nano-constrictions by electrical breakdown. *AIP Advances* **2022**, *12* (5), 055312.

(4) Yan, J.; Zhang, Y.; Kim, P.; Pinczuk, A. Electric Field Effect Tuning of Electron-Phonon Coupling in Graphene. *Physical Review Letters* **2007**, *98* (16), 166802.

(5) Das, A.; Pisana, S.; Chakraborty, B.; Piscanec, S.; Saha, S. K.; Waghmare, U. V.; Novoselov, K. S.; Krishnamurthy, H. R.; Geim, A. K.; Ferrari, A. C.; et al. Monitoring dopants by Raman scattering in an electrochemically top-gated graphene transistor. *Nature Nanotechnology* **2008**, *3* (4), 210-215.

(6) Jnawali, G.; Rao, Y.; Beck, J. H.; Petrone, N.; Kymissis, I.; Hone, J.; Heinz, T. F. Observation of Ground- and Excited-State Charge Transfer at the C60/Graphene Interface. *ACS Nano* **2015**, *9* (7), 7175-7185.
(7) Pirkle, A.; Chan, J.; Venugopal, A.; Hinojos, D.; Magnuson, C. W.; McDonnell, S.; Colombo, L.; Vogel, E. M.; Ruoff, R. S.; Wallace, R. M. The effect of chemical residues on the physical and electrical properties of chemical vapor deposited graphene transferred to SiO2. *Appl. Phys. Lett.* **2011**, *99* (12), 122108.
(8) Thodkar, K.; Thompson, D.; Lüönd, F.; Moser, L.; Overney, F.; Marot, L.; Schönenberger, C.; Jeanneret, B.; Calame, M. Restoring the Electrical Properties of CVD Graphene via Physisorption of Molecular Adsorbates. *ACS Appl. Mater. Interfaces* **2017**, *9* (29), 25014-25022.
(9) Lee, W. H.; Park, J.; Sim, S. H.; Lim, S.; Kim, K. S.; Hong, B. H.; Cho, K. Surface-Directed Molecular Assembly of Pentacene on Monolayer Graphene for High-Performance Organic Transistors. *Journal of the American Chemical Society* **2011**, *133* (12), 4447-4454.
(10) Berke, K.; Tongay, S.; Mccarthy, M. A.; Rinzler, A. G.; Appleton, B. R.; Hebard, A. F. Current transport across the pentacene/CVD-grown graphene interface for diode applications. *J Phys Condens Matter* **2012**, *24* (25), 255802.
(11) Ojeda-Aristizabal, C.; Bao, W.; Fuhrer, M. S. Thin-film barristor: A gate-tunable vertical graphene-pentacene device. *Phys. Rev. B* **2013**, *88* (3), 035435.
(12) Hwang, W. T.; Min, M.; Jeong, H.; Kim, D.; Jang, J.; Yoo, D.; Jang, Y.; Kim, J. W.; Yoon, J.; Chung, S.; et al. Gate-dependent asymmetric transport characteristics in pentacene barristors with graphene electrodes. *Nanotechnology* **2016**, *27* (47), 475201.
(13) Kim, J. S.; Choi, Y. J.; Woo, H. J.; Yang, J.; Song, Y. J.; Kang, M. S.; Cho, J. H. Schottky-Barrier-Controllable Graphene Electrode to Boost Rectification in Organic Vertical P-N Junction Photodiodes. *Advanced Functional Materials* **2017**, *27* (48), 1704475.
(14) Tongay, S.; Lemaitre, M.; Miao, X.; Gila, B.; Appleton, B. R.; Hebard, A. F. Rectification at Graphene-Semiconductor Interfaces: Zero-Gap Semiconductor-Based Diodes. *Physical Review X* **2012**, *2* (1), 011002.
(15) Di Bartolomeo, A. Graphene Schottky diodes: An experimental review of the rectifying graphene/semiconductor heterojunction. *Physics Reports* **2016**, *606*, 1-58.
(16) Hwang, W.-T.; Min, M.; Jeong, H.; Kim, D.; Jang, J.; Yoo, D.; Jang, Y.; Kim, J.-W.; Yoon, J.; Chung, S.; et al. Gate-dependent asymmetric transport characteristics in pentacene barristors with graphene electrodes. *Nanotechnology* **2016**, *27* (47), 475201.

(17) Cui, X. D.; Primak, A.; Zarate, X.; Tomfohr, J.; Sankey, O. F.; Moore, A. L.; Moore, T. A.; Gust, D.; Harris, G.; Lindsay, S. M. Reproductible measurement of single-molecule conductivity. *Science* **2001**, *294*, 571-574.

(18) Cui, X. D.; Zarate, X.; Tomfohr, J.; Sankey, O. F.; Primak, A.; Moore, A. L.; Moore, T. A.; Gust, D.; Harris, G.; Lindsay, S. M. Making electrical contacts to molecular monolayers. *Nanotechnology* **2002**, *13*, 5-14.

(19) Engelkes, V. B.; Daniel Frisbie, C. Simultaneous nanoindentation and electron tunneling through alkanethiol self-assembled monolayers. *The Journal of Physical Chemistry B* **2006**, *110* (20), 10011-10020.

(20) Morita, T.; Lindsay, S. Determination of Single Molecule Conductances of Alkanedithiols by Conducting-Atomic Force Microscopy with Large Gold Nanoparticles. *J Am Chem Soc* **2007**, *129* (23), 7262-7263.

(21) Johnson, K. L. *Contact Mechanics*; Cambridge University Press, 1987.

(22) Tahk, D.; Lee, H. H.; Khang, D.-Y. Elastic Moduli of Organic Electronic Materials by the Buckling Method. *Macromolecules* **2009**, *42* (18), 7079-7083.

(23) Root, S. E.; Savagatrup, S.; Printz, A. D.; Rodriquez, D.; Lipomi, D. J. Mechanical Properties of Organic Semiconductors for Stretchable, Highly Flexible, and Mechanically Robust Electronics. *Chemical Reviews* **2017**, *117* (9), 6467-6499.

(24) Perrin, M. L.; Frisenda, R.; Koole, M.; Seldenthuis, J. S.; Gil, J. A.; Valkenier, H.; Hummelen, J. C.; Renaud, N.; Grozema, F. C.; Thijssen, J. M.; et al. Large negative differential conductance in single-molecule break junctions. *Nat Nanotechnol* **2014**, *9* (10), 830-834.

(25) Perrin, M. L.; Doelman, M.; Eelkema, R.; van der Zant, H. S. J. Design of an efficient coherent multi-site single-molecule rectifier. *Phys Chem Chem Phys* **2017**, *19* (43), 29187-29194.

(26) Feenstra, R. M.; Jena, D.; Gu, G. Single-particle tunneling in doped graphene-insulator-graphene junctions. *Journal of Applied Physics* **2012**, *111* (4), 043711.

(27) Datta, S. Electronic transport in mesoscopic systems; Cambridge University Press, 1995.

(28) Cuevas, J. C.; Scheer, E. Molecular Electronics: An introduction to theory and experiment; World Scientific, 2010.

(29) Amirav, L.; Wachtler, M. Nano Schottky? *Nano Lett* **2022**, *22*, 9783-9785.